







RESEARCH ARTICLE | AUGUST 12 2025

Quantifying the change in optical absorption caused by the ferro- to paraelectric transition in Sm-substituted BiFeO₃ powders

Special Collection: [Ferroic Materials, Domains, and Domain Walls: Bridging Fundamentals with Next-Generation Technology](#)

Christina Hill ; Michele Melchiorre ; Cosme Milesi-Brault ; Pascale Gemeiner; Fabienne Karolak; Christine Bogicevic; Brahim Dkhil ; Ingrid Cañero-Infante ; Mael Guennou 



J. Appl. Phys. 138, 064103 (2025)

<https://doi.org/10.1063/5.0275086>



Articles You May Be Interested In

Ferro-ionic states and domains morphology in Hf_xZr_{1-x}O₂ nanoparticles

J. Appl. Phys. (January 2025)

Mapping the structural transitions controlled by the trilinear coupling in Ca_{3-x}Sr_xTi₂O₇

J. Appl. Phys. (June 2019)

Micro-Raman scattering and dielectric investigations of phase transitions behavior in the PbHf_{0.7}Sn_{0.3}O₃ single crystal

J. Appl. Phys. (September 2017)



Nanotechnology & Materials Science



Optics & Photonics



Impedance Analysis



Scanning Probe Microscopy



Sensors



Failure Analysis & Semiconductors



Unlock the Full Spectrum.
From DC to 8.5 GHz.

Your Application. Measured.

[Find out more](#)

 Zurich Instruments

Quantifying the change in optical absorption caused by the ferro- to paraelectric transition in Sm-substituted BiFeO₃ powders

Cite as: J. Appl. Phys. 138, 064103 (2025); doi: 10.1063/5.0275086

Submitted: 10 April 2025 · Accepted: 21 July 2025 ·

Published Online: 12 August 2025



Christina Hill,^{1,2,3,a)} Michele Melchiorre,¹ Cosme Milesi-Brault,⁴ Pascale Gemeiner,⁴ Fabienne Karolak,⁴ Christine Bogicevic,⁴ Brahim Dkhil,⁴ Ingrid Cañero-Infante,⁵ and Mael Guennou^{1,3}

AFFILIATIONS

¹Department of Physics and Materials Science, University of Luxembourg, 41 rue du Brill, 4422 Belvaux, Luxembourg

²Luxembourg Institute of Science and Technology, 41 rue du Brill, 4422 Belvaux, Luxembourg

³Inter-institutional Research Group Uni.lu—LIST on Ferroic Materials, 41 rue du Brill, 4422 Belvaux, Luxembourg

⁴Université Paris-Saclay, CNRS, CentraleSupélec, Laboratoire SPMS, 91190 Gif-sur-Yvette, France

⁵Université de Lyon, Institut des Nanotechnologies de Lyon, CNRS UMR 5270 ECL INSA UCBL CPE, 1 rue Enrico Fermi, F-69621 Villeurbanne, France

Note: This paper is part of the Special Topic, Ferroic Materials, Domains, and Domain Walls: Bridging Fundamentals with Next-Generation Technology.

^{a)}Author to whom correspondence should be addressed: christina.hill@uni.lu

ABSTRACT

The substitution of bismuth by samarium in BiFeO₃ is known to induce a structural phase transition from the polar phase to a non-polar phase, with a possible antiferroelectric intermediate structure. In this paper, we investigate the impact of this phase change on the optical properties. The optical bandgap was measured by diffuse reflectance as a function of temperature for several samarium concentrations across the structural phase transition. We found that the optical bandgap for each of the pure phases varies linearly with temperature and that the phase transitions are revealed by smooth transitions between those linear regimes. This allows us to quantify the contribution of the structural change in the optical absorption. We find that a difference in optical bandgap of about ≈ 130 meV can be attributed to the phase change. We anticipate that the same change could be obtained by applying an electric field in an antiferroelectric composition.

© 2025 Author(s). All article content, except where otherwise noted, is licensed under a Creative Commons Attribution (CC BY) license (<https://creativecommons.org/licenses/by/4.0/>). <https://doi.org/10.1063/5.0275086>

INTRODUCTION

Bismuth ferrite BiFeO₃ (BFO) is a pivotal compound in materials science as a model multiferroic crystal combining ferroelectric properties at room temperature and complex magnetic order. Due to a bandgap energy in the visible light range at ≈ 2.4 eV, BFO has attracted considerable attention for potential use in photocatalytic^{1–3} and photovoltaic^{4–8} applications. Pure BFO crystallizes in a rhombohedral structure with space group *R3c* and undergoes a first-order phase transition to a paraelectric phase at 1100 K. The substitution of bismuth by a rare-earth element *R* has attracted attention for a long time as a way to tune the structural⁹ and optical properties of BFO.^{10–12} At sufficiently high *R*

concentrations, the compound stabilizes in an orthorhombic non-polar *Pnma* crystal structure that is also the structure of the pure rare-earth orthoferrites *R*FeO₃ and of the high-temperature paraelectric phase of BFO. The transition between the polar *R3c* phase (at low *x*) and the non-polar *Pnma* phase (at high *x*) occurs not only via phase coexistence but also, in a narrow composition range, via intermediate bridging phases usually characterized by non-polar structures, larger unit cells, and antipolar cation orderings. These intermediate phases are strongly reminiscent of—when not identical to—the centrosymmetric *Pbam* crystal structure of the model antiferroelectric perovskite PbZrO₃, and are therefore very often described as antiferroelectric, even though actual antiferroelectric

14 October 2025 09:20:51

switching, i.e., the transition induced by an electric field, is difficult to observe due to the generally leaky character of BFO-based compounds and has been reported only in few studies.^{13,14}

In this paper, we investigate the optical properties of rare-earth substituted BiFeO₃ systems at the ferroelectric–paraelectric phase transition. We focus on samarium-substituted BiFeO₃ (SmBFO) as a model system. Samarium has an ionic radius significantly smaller than bismuth (1.079 Å vs 1.17 Å), so the chemical pressure effect is quite drastic. Structural studies on powders^{15,16} and ceramics^{9,17,18} report some degree of phase coexistence between $x \approx 8\%$ and $x \approx 20\%$, with a fraction of intermediate PbZrO₃-like phase peaking at $x \approx 15\%$. It is also the composition where AFE-like double hysteresis loops have been reported in thin films.^{13,19} Overall, it appears that the details of the phases in the morphotropic region are complex, and their stabilization is sensitive to the processing route and the history of the samples. Optical studies at room temperature have shown that Sm-substitution causes a shift of the optical bandgap toward lower energies in the polar phase and across the morphotropic region.^{10,20–25} However, the literature presents a wide range of values regarding this shift. For instance, Orudzhev *et al.* found a difference of 100 meV²⁵ from pure BFO *R3c* structures to the Sm 20% *Pnma* structure while Kebede *et al.* found a difference of 410 meV.²³ The role of the phase transition in the optical absorption remains unclear, and variations in optical absorption could potentially arise from other factors such as changes in volume, atomic distortion, even in the absence of structural changes.

The purpose of this paper is to quantify the variation in the optical absorption by the structural change from the ferro- to the paraelectric phase in Sm-substituted BFO. The motivation is to clarify the role of the phase transition as a tuning mechanism. This is relevant for tuning the optical properties by controlling the phase fractions in the morphotropic region. It is also important to evaluate the possibility to tune the optical absorption by inducing the phase transition with an electric field for antiferroelectric compositions, i.e., to evaluate the electrochromic properties of SmBFO. To do so, we performed measurements of optical properties as a function of temperature for several compositions across the morphotropic region. We demonstrate that this approach enables us to estimate the role of the structural transition in the change of the optical bandgap. The origin of this change is discussed.

EXPERIMENTAL DETAILS

Powders of Sm-substituted BiFeO₃ (Sm_{*x*}Bi_{1–*x*}FeO₃ with $x = 10, 12, 14, 16, 18$ and 20%) were processed starting from the high quality oxides Sm₂O₃ from ChemPur, Bi₂O₃ from Alfa Aesar and Fe₂O₃ from Ventron by mechanochemical synthesis using a ball milling process. We used the PM100 miller from Verder. The starting oxides were mixed in a 125 ml ZrO₂ jar with 100 mm ZrO₂ grinding balls, then rotated for 24 h, alternating between 2 min rotation and 2 min break, resulting in effective rotation of 8 h and 8 h of break.

For each composition, powders and pellets have been processed. The powders were annealed at 850 °C. Pellets of 8 mm in diameter were pressed with a uniaxial pressure of 150 MPa. The pellets were then sintered at 850 °C at an atmospheric pressure of

1/2Al₂O₃+1/2Bi₂O₃ using a temperature ramp of 350 °C /h for 6 h. The phase purity and sample quality have been checked at room temperature by x-ray diffraction (XRD) on a D2 Bruker diffractometer using Cu K_α radiation and by Raman spectroscopy with a LabRam system from Horiba with a 633 nm laser, a laser power of 1 mW, and a laser spot size of 1.2 μm in diameter. The particle distribution and morphology was studied by a SEM field-emission gun Hitachi SU-70. All compositions show a faceted morphology and an average particle size of ≈ 400 nm (see Fig. S1 in the [supplementary material](#)). A chemical analysis using energy dispersive x-ray (EDX) spectroscopy with the TEM JEOL JEM-F2000 confirms the presence of bismuth (Bi), iron (Fe), samarium (Sm), and oxygen. The variation in Sm concentration is reflected in the gradual increase of the relative intensities of the Sm peaks, as shown in Fig. S2 of the [supplementary material](#). EDX maps confirm a homogeneous distribution of the elements across all samples.

Raman and XRD measurements at room temperature overall confirm results known from the literature with a pure *R3c* phase for low Sm concentrations (10% and 12%) and a pure *Pnma* phase for high Sm concentrations (20%). Phase coexistence is observed for the intermediate Sm concentrations (14%, 16%, and 18%); see Fig. S3 in the [supplementary material](#). Some very small peaks were occasionally observed that could indicate the presence of either the intermediate *Pbam* phase or possibly a spurious phase, but in such small amounts that they do not affect the average provided by optical measurements. Besides, the Raman spectra did not give any evidence for any other phase than the *R3c* phase and the *Pnma* phase (Fig. S4 in the [supplementary material](#)), in spite of the general sensitivity of Raman spectroscopy. As a result, in the following, we will discuss the data considering only the *R3c* phase, the *Pnma* phase, and a mixture of both.

The optical properties were investigated by diffuse reflectance on powders in the UV–visible range using a PerkinElmer Lambda 850 equipped with a Harrick Praying Mantis diffuse reflectance accessory. The diffuse reflectance was measured across the phase transition for increasing- and decreasing-temperature runs up to 800 K for all Sm compositions. A BaSO₄ powder without absorption in the spectral range of interest was used as a reference for the total reflectance. The focused beam spot size was about 2 mm².

We analyze the diffuse reflectance using Kubelka–Munk theory, neglecting specular reflectance.²⁶ The Kubelka–Munk theory is a two-flux model with differential equation formalism using empirical coefficients to describe the scattering and absorption of light in a continuous medium. The Kubelka–Munk function $F(R_\infty)$ is given by the following equation with R_∞ being the diffuse reflectance, α' the Kubelka–Munk absorption constant, and s the Kubelka–Munk scattering constant,^{27–29}

$$F(R_\infty) = \frac{\alpha'}{s} = \frac{(1 - R_\infty)^2}{2R_\infty} \approx \alpha.$$

The Kubelka–Munk formalism assumes an infinitely thick sample and s to be independent of the wavelength of the incident light. In this case, $F(R_\infty)$ is proportional to the absorption coefficient α .²⁹

RESULTS AND DISCUSSION

Diffuse reflectance spectra at room temperature

The diffuse reflectance spectra for all compositions are qualitatively comparable to those previously described for pure BFO powders.³⁰ Figure 1 shows the absorption spectra for the different compositions derived from the Kubelka–Munk formalism from the diffuse reflectance measurements presented in Fig. S5 in the [supplementary material](#). For comparison purposes, each absorption spectrum is normalized to the absorption peak at 2.5 eV above the bandgap. The absorption spectra show several features. The most remarkable is the sharp and sudden increase around 2 eV, a typical feature of a band-to-band transition. This is associated with the bandgap of the material. At lower energies, the function exhibits weak bumps around 1.5 and 1.9 eV that are associated with Fe^{3+} d - d excitations.^{30–32} At higher energies, broad absorption bands are visible at 3.4 and 5.2 eV and a narrow band at 2.5 eV that can be associated with higher electronic transitions.³⁰

With such a complex absorption profile, it is not obvious how to determine the bandgap. The presence of important absorption tails below the bandgap precludes the use of classical Tauc plots. We choose here to define the optical bandgap as the inflection point in the absorption edge as presented in Ref. 33. In this way, we are not sensitive to the details of the absorption spectrum, including the direct or indirect nature of the gap, and we do not depend on an arbitrary choice for a linear extrapolation in a Tauc plot. This also

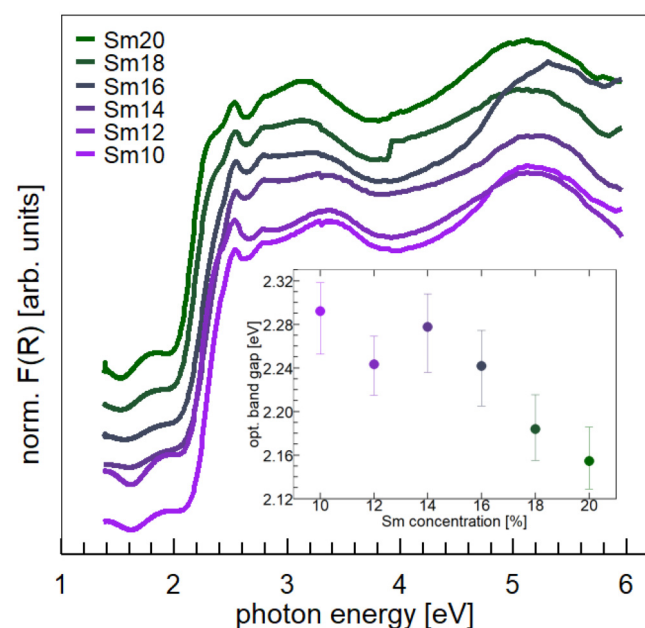


FIG. 1. Room temperature absorption spectra derived from the reflectance spectra using the Kubelka–Munk formalism. Spectra are normalized to the absorption peak at 2.5 eV slightly above the optical bandgap and stacked to facilitate better comparison. The inset shows the decreasing general trend of the optical bandgap energy with increasing Samarium concentration.

provides us with a way to treat consistently the temperature-dependent data. The inset of Fig. 1 shows the optical bandgap as a function of the Sm concentration. The error bars reflect the energy range where the first derivative of the edge is greater than 95% of its maximum value, which allows for some uncertainty in the location of the inflection point and more importantly shows that the precision of the method is similar for all samples. Overall, we observe that the bandgap energy decreases with increasing Sm concentration, as observed in Refs. 20, 22, 23, and 25.

For Sm concentration of 10%, we found a bandgap energy of 2.3 eV. In the literature, the bandgap energies for the same composition ranged from 2.06 eV^{22,23} to 2.26 eV,²⁰ with one study reporting a value of 2.13 eV.²⁵ In all of these studies, measurements were performed on nanoparticles for which a strong size dependence on the optical properties is known³⁰ and the bandgap energy was extracted using a Tauc plot. The large variations in the bandgap energy from one work to the other result from variations in particle size and the challenge of consistently determining the bandgap energy through the Tauc plot.

In the next step, we aim to investigate the temperature dependence of both absorption and the optical bandgap.

Optical bandgap as a function of temperature

All powders were measured by diffuse reflectance at high temperatures, both increasing- and decreasing-temperature runs being recorded. As a representative example, we show the absorption spectra derived from the diffuse reflectance measured at the increasing-temperature run for the composition of $x = 14\%$ in Fig. 2. The absorption spectra for all other compositions are shown in Fig. S6 in the [supplementary material](#). The absorption edge,

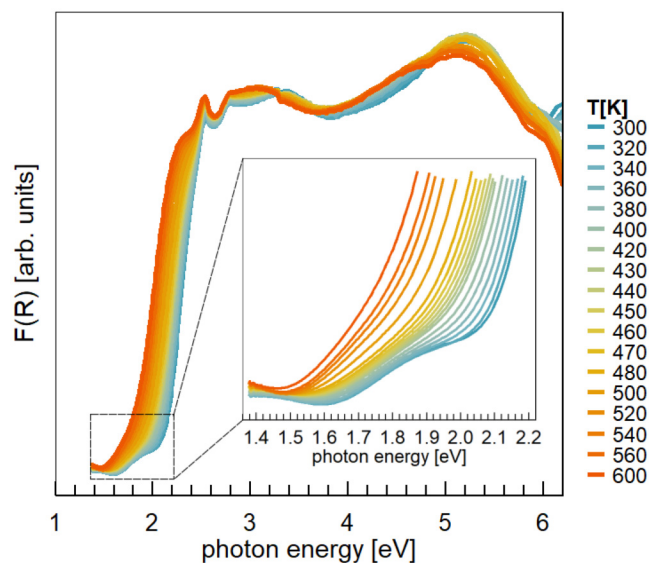


FIG. 2. Absorption spectra derived from the diffuse reflectance measured at the increasing-temperature run for the powder $(\text{Bi}_{0.86}\text{Sm}_{0.14})\text{FeO}_3$ using Kubelka–Munk functions $F(R)$. The inset shows a zoom on the low energy tails.

indicated by a sudden increase in absorption, is found around 2 eV and strongly shifts with temperature, as expected from studies on BFO single crystals.^{34,35} The weak absorption features below the absorption edge seem to disappear with increasing temperatures, see the inset of Fig. 2. Qualitatively similar observations were made for all compositions.

For every run, we extracted the optical bandgap, i.e., the inflection point in the absorption edge, from the Kubelka–Munk functions $F(R)$ of all compositions for both the increasing- and decreasing-temperature runs. The results are shown in Fig. 3. The blue triangles pointing up show the optical bandgap from the increasing-temperature run, while the brown triangles pointing down represent the optical bandgap from the decreasing-temperature run.

For the two highest concentrations of Sm 18% and 20%, the optical bandgap energy decreases linearly with temperature and does not show any anomaly, meaning that there is no indication for a structural phase transition.

In all other cases, deviations from linearity are clearly visible. The most representative case is obtained for 14% that shows two linear behaviors, one at low temperatures and one at high temperatures. In between, the bandgap shows an inflection that we associated with the phase transition between the low-temperature polar $R3c$ phase and the high-temperature non-polar $Pnma$ phase. This change occurs smoothly over a wide temperature range of ≈ 150 K. There is a very clear hysteresis between the increasing- and decreasing-temperature runs. The transition temperature, given by the inflection in the optical bandgap, is ≈ 50 K lower for the decreasing-temperature run than for the increasing-temperature run. The presence of an hysteresis and the coexistence of phases are consistent with the first-order character of the rhombohedral to orthorhombic transition.

The other compositions show the same scenario, whereby the transition is shifted toward lower temperatures for higher Sm concentrations. For the highest concentrations of 18% and 20% Sm, no transition is observable within the measured temperature range; it would be expected to occur below room temperature. For 10% Sm, the transition is only partially observed. Although we observe the onset of the transition and some hysteretic behavior, the maximum temperature of 800 K is not sufficient to reach the high-temperature linear behavior. The hysteresis is of practical importance for the preparation of samples at room temperature in the 16%–18% range that will depend strongly on the thermal history of the sample.

We fitted the linear regions of the bandgap for Sm concentrations of 10% and 20%. The fits are shown as solid lines. Interestingly, comparing the slopes of the low-temperature and the high-temperature phase, the value is nearly identical with ≈ -0.49 meV K⁻¹. For the intermediate compositions where the linear regime is not as broad, we fixed the slope, using the slope of the fit for 10% Sm for low temperatures and the slopes of the fits for 20% Sm for high temperatures. These fits are represented by dashed lines. We believe that it is reasonable to assume that the slope must be identical from one composition to another, provided that the dominant phase is the same.

The value -0.49 meV K⁻¹ is two to three times slower than for pure BFO with ≈ -1.3 meV K⁻¹.³⁴ However, when measured at the inflection point where the slope is maximum and the change

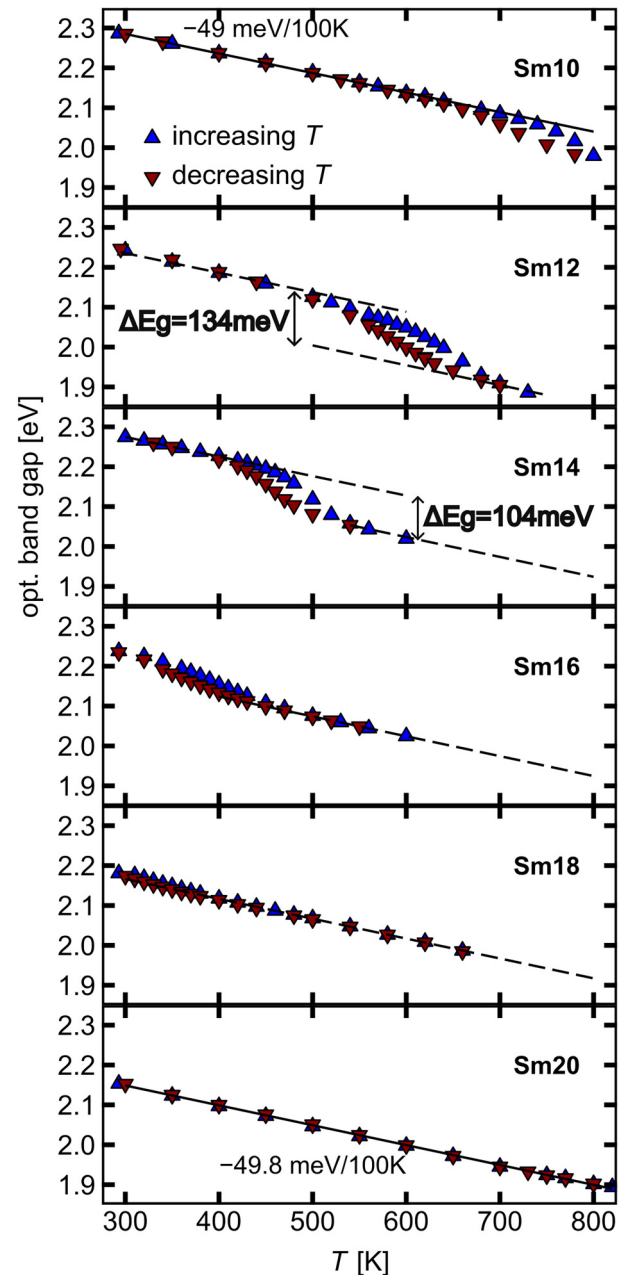


FIG. 3. Optical bandgap defined as the inflection point in the absorption edge of the Kubelka–Munk function $F(R)$ vs temperature for $(\text{Bi}_{1-x}\text{Sm}_x)\text{FeO}_3$ for x varying from 10 % to 20 % upon increasing- and decreasing-temperature runs. Solid lines are linear fits to the data. For the fits indicated by dashed lines, the slope from low (high) temperatures and low (high) Sm concentrations was carried over.

mostly driven by the phase transition, it reaches -1.7 and -2.05 meV K⁻¹ for 12% and 14%, respectively, which highlights the strong contribution of the phase transition in this evolution. For 12% and 14% Sm, we calculated the difference between the

low-temperature and high-temperature linear fits, as a way to eliminate the effect of temperature and thermal expansion and isolate the contribution of the structural phase change. This results in values of ΔE_g of 134 and 104 meV, respectively. The smaller value for 14% Sm is attributed to the fact that the phase transition is not complete and the sample still displays some degree of phase coexistence even at room temperature, as seen in XRD and discussed in the next section. We, therefore, retain 12% Sm as the sample that is closest to a pure *R3c* to pure *Pnma* transition in the investigated temperature range, and 134 meV as the difference in optical bandgap attributed to this phase transition.

This value closely aligns with the variation in the optical bandgap of 200 meV from rhombohedral to supertetragonal found in strained BFO thin films.³⁶ Considering that the engineered strain in this example is much larger than the strain introduced by the phase transition in our material system, it is reasonable to assume that the change in the optical bandgap is directly proportional to the strain. We also note that our value is very close to the 130 meV reported for the comparison between the paraelectric cubic phase and the ferroelectric tetragonal phase in PbTiO_3 .³⁷

Phase diagram

Finally, we tentatively construct a phase diagram from the optical data, as shown in Fig. 4. We assume a pure phase where the optical bandgap behaves linearly with temperature and a mixture of phases at temperatures where we observe a significant deviation (± 5 meV) from linearity. The diagram is constructed using data collected upon increasing temperature. We can distinctly identify three regions: the polar *R3c* phase at low temperatures and low Sm concentrations, the non-polar *Pnma* phase at high temperatures and high Sm concentrations, and a mixture of both phases in between.

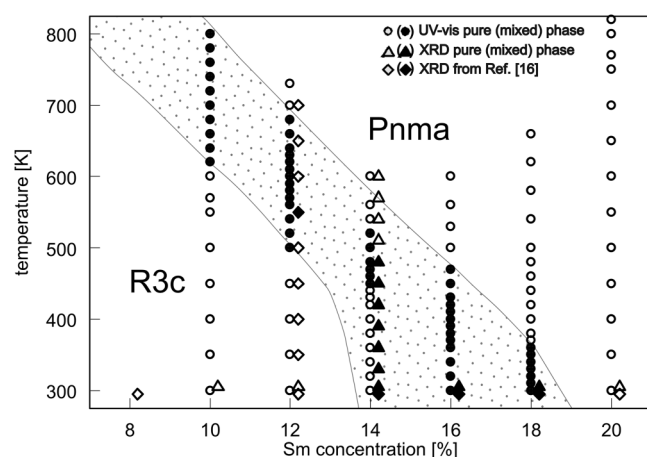


FIG. 4. Phase diagram constructed using optical data (circles) and XRD data (triangles), supplemented by XRD data from the literature¹⁶ (diamonds). For clarity, the XRD data points are slightly shifted with respect to the exact Sm concentration. Open symbols indicate a pure phase (*R3c* or *Pnma*) and filled symbols are data points where phase coexistence is observed.

The so constructed phase diagram can be complemented by previously reported XRD measurements,¹⁶ as well as our own XRD data at room temperature. Both the literature and our XRD data confirm the presence of a pure *R3c* phase at room temperature for low Sm concentrations ranging from 8% to 12%. A pure *Pnma* phase is found for the highest Sm concentration of 20%. Near the phase transition, we observe the coexistence of the two phases. 14% appears as a limiting case where phase coexistence is not immediately apparent from the optical data but is seen in XRD at room temperature. For clarification, we also carried out complementary XRD measurements as a function of temperature up to 800 K with increasing- and decreasing-temperature runs; see Fig. S7 in the [supplementary material](#). This experiment confirms the coexistence of both phases at room temperature, including after cooling down. The presence of phase coexistence is also consistent with the smaller ΔE_g measured for 14% as compared to 12%.

Overall, both optical and XRD data exhibit the same trends, but with differences in the range where phase coexistence is observed. In the optical data, the range for phase coexistence appears significantly broader in temperature. For 12% Sm concentration, as temperature increases, the literature reports a phase transition accompanied by phase coexistence at 550 K. This could also originate from the different length scales probed by the two techniques. While XRD gives a volume average, diffuse reflectance is a highly surface sensitive technique. This, combined with the famous skin effect of BFO and BFO-based materials, may lead to differences observed in phase coexistence and apparent transition temperatures.

CONCLUSION

In summary, this paper shows an optical study of BiFeO_3 powders modified by Sm-substitution with a concentration ranging from 10% to 20% across the morphotropic region. We have shown that the optical bandgap extracted by diffuse reflectance and its treatment via the Kubelka-Munk function reveal the expected phase transition between the polar BFO-like phase and the non-polar orthorhombic phase at high Sm concentrations and high temperatures. The phase diagram established from optical data appears to be in qualitative agreement with the known behavior of these solid solutions, but it is also characterized by a very large hysteresis of the transition temperature. We estimated that the phase transition comes with a shift in the bandgap of about 130 meV, which we primarily attribute to the difference in volume strain between the two phases. In the context of a possible antiferroelectric behavior of SmBFO , we anticipate that this value gives a good estimation of the expected bandgap variation as the non-polar to polar transition is induced by an electric field, i.e., a good estimation of its potential electrochromic performance.

SUPPLEMENTARY MATERIAL

See the [supplementary material](#) for (I) grain size and morphology (SEM analysis); (II) Energy-dispersive X-ray spectroscopy (EDX); (III) XRD patterns at room temperature; (IV) composition-dependent Raman analysis; (V) composition-dependent diffuse reflectance measurements; (VI) absorption as a function of temperature for different compositions; (VII) temperature-dependent XRD analysis for a Sm concentration of 14%.

14 October 2025 09:20:51

ACKNOWLEDGMENTS

C.H. acknowledges funding from the Fond National de la Recherche under Project No. PRIDE/15/10935404. C.M.-B. acknowledges funding from the Fond National de la Recherche under Project BIAFET C16/MS/1134912/Guennou. B.D. acknowledges funding from the Fond National de la Recherche under Project INTER/MOBILITY/19/13992074 and the French National Research Agency (ANR) through Nos. CERACOO ANR-23-CE05-0012, SOFIANE ANR-23-CE09-0007, and PHOTOTRICS ANR-24-CE08-0954-03.

AUTHOR DECLARATIONS

Conflict of Interest

The authors have no conflicts to disclose.

Author Contributions

Christina Hill: Conceptualization (supporting); Formal analysis (lead); Visualization (lead); Writing – original draft (lead); Writing – review & editing (lead). **Michele Melchiorre:** Data curation (supporting). **Cosme Milesi-Brault:** Data curation (equal); Formal analysis (equal); Validation (equal); Writing – review & editing (equal). **Pascal Gemeiner:** Data curation (equal); Formal analysis (equal); Writing – review & editing (equal). **Fabienne Karolak:** Data curation (equal); Investigation (equal). **Christine Bogicevic:** Data curation (equal); Investigation (equal). **Brahim Dkhil:** Conceptualization (equal); Funding acquisition (equal); Validation (equal); Writing – review & editing (equal). **Ingrid Cañero-Infante:** Conceptualization (equal); Validation (equal); Writing – review & editing (equal). **Mael Guennou:** Conceptualization (lead); Funding acquisition (lead); Resources (equal); Supervision (equal); Validation (equal); Writing – original draft (equal); Writing – review & editing (equal).

DATA AVAILABILITY

The data that support the findings of this study are openly available in Zenodo at [10.5281/zenodo.15175369](https://doi.org/10.5281/zenodo.15175369), Ref. 38.

REFERENCES

- ¹S. Irfan, Z. Zhuanghao, F. Li, Y.-X. Chen, G.-X. Liang, J.-T. Luo, and F. Ping, “Critical review: Bismuth ferrite as an emerging visible light active nanostructured photocatalyst,” *J. Mater. Res. Technol.* **8**, 6375 (2019).
- ²S. Supriya, “Recent trends and morphology mechanisms of rare-earth based BiFeO₃ nano perovskites with excellent photocatalytic performances,” *J. Rare Earths* **41**, 331 (2023).
- ³W. Amdouni, M. Fricaudet, M. Otoničar, V. Garcia, S. Fusil, J. Kreisel, H. Maghraoui-Meherzi, and B. Dkhil, “BiFeO₃ nanoparticles: The ‘holy-grail’ of piezo-photocatalysts?” *Adv. Mater.* **35**, 2301841 (2023).
- ⁴T. Choi, S. Lee, Y. J. Choi, V. Kiryukhin, and S.-W. Cheong, “Switchable ferroelectric diode and photovoltaic effect in BiFeO₃,” *Science* **324**, 63 (2009).
- ⁵S. Y. Yang, L. W. Martin, S. J. Byrnes, T. E. Conry, S. R. Basu, D. Paran, L. Reichertz, J. Ihlefeld, C. Adamo, A. Melville, Y.-H. Chu, C.-H. Yang, J. L. Musfeldt, D. G. Schlom, J. W. Ager III, and R. Ramesh, “Photovoltaic effects in BiFeO₃,” *Appl. Phys. Lett.* **95**, 062909 (2009).
- ⁶G. S. Lotey and N. K. Verma, “Gd-doped BiFeO₃ nanoparticles—A novel material for highly efficient dye-sensitized solar cells,” *Chem. Phys. Lett.* **574**, 71 (2013).
- ⁷D. Tiwari, D. J. Fermin, T. K. Chaudhuri, and A. Ray, “Solution processed bismuth ferrite thin films for all-oxide solar photovoltaics,” *J. Phys. Chem. C* **119**, 5872 (2015).
- ⁸L. You, F. Zheng, L. Fang, Y. Zhou, L. Z. Tan, Z. Zhang, G. Ma, D. Schmidt, A. Rusydi, L. Wang, L. Chang, A. M. Rappe, and J. Wang, “Enhancing ferroelectric photovoltaic effect by polar order engineering,” *Sci. Adv.* **4**, eaat3438 (2018).
- ⁹D. C. Arnold, “Composition-driven structural phase transitions in rare-earth-doped BiFeO₃ ceramics: A review,” *IEEE Trans. Ultrasonics Ferroelectrics Frequency Control* **62**, 62 (2015).
- ¹⁰S. Irfan, Y. Shen, S. Rizwan, H.-C. Wang, S. B. Khan, and C.-W. Nan, “Band-gap engineering and enhanced photocatalytic activity of Sm and Mn doped BiFeO₃ nanoparticles,” *J. Am. Ceram. Soc.* **100**, 31 (2017).
- ¹¹F. Mumtaz, S. Nasir, G. Jaffari, and S. Shah, “Chemical pressure exerted by rare earth substitution in BiFeO₃: Effect on crystal symmetry, band structure and magnetism,” *J. Alloys Compd.* **876**, 160178 (2021).
- ¹²A. Gholizadeh and S. Hosseini, “Effect of heavy rare-earth substitution on physical properties of BiFeO₃ thin films and their photocatalytic application,” *J. Am. Ceram. Soc.* **107**, 4209 (2024).
- ¹³D. Kan, C.-J. Cheng, V. Nagarajan, and I. Takeuchi, “Composition and temperature-induced structural evolution in La, Sm, and Dy substituted BiFeO₃ epitaxial thin films at morphotropic phase boundaries,” *J. Appl. Phys.* **110**, 014106 (2011).
- ¹⁴J. A. Mundy, B. F. Grosso, C. A. Heikes, D. Ferenc Segedin, Z. Wang, Y.-T. Shao, C. Dai, B. H. Goodge, Q. N. Meier, C. T. Nelson, B. Prasad, F. Xue, S. Ganschow, D. A. Muller, L. F. Kourkoutis, L.-Q. Chen, W. D. Ratcliff, N. A. Spaldin, R. Ramesh, and D. G. Schlom, “Liberating a hidden antiferroelectric phase with interfacial electrostatic engineering,” *Sci. Adv.* **8**, eabg5860 (2022).
- ¹⁵A. Pakalniškis, R. Skaudžius, D. V. Zhaludkevich, A. L. Zhaludkevich, D. O. Alikin, A. S. Abramov, T. Murauskas, V. Y. Shur, A. A. Dronov, M. V. Silibin, A. Selskis, R. Ramanauskas, A. Lukowiak, W. Strek, D. V. Karpinsky, and A. Kareiva, “Morphotropic phase boundary in Sm-substituted BiFeO₃ ceramics: Local vs microscopic approaches,” *J. Alloys Compd.* **875**, 159994 (2021).
- ¹⁶A. Pakalniškis, R. Skaudžius, D. V. Zhaludkevich, S. I. Latushka, V. Sikolenko, A. V. Sysa, M. Silibin, K. Mažeika, D. Baltrūnas, G. Niaura, M. Talaikis, D. V. Karpinsky, and A. Kareiva, “Pressure induced phase transitions in Sm-doped BiFeO₃ in the morphotropic phase boundary,” *Mater. Chem. Phys.* **277**, 125458 (2022).
- ¹⁷X. X. Shi, X. Q. Liu, and X. M. Chen, “Structure evolution and piezoelectric properties across the morphotropic phase boundary of Sm-substituted BiFeO₃ ceramics,” *J. Appl. Phys.* **119**, 064104 (2016).
- ¹⁸C. Yu, G. Viola, D. Zhang, K. Zhou, V. Koval, A. Mahajan, R. M. Wilson, N. V. Tarakina, I. Abrahams, and H. Yan, “Phase evolution and electrical behaviour of samarium-substituted bismuth ferrite ceramics,” *J. Eur. Ceram. Soc.* **38**, 1374 (2018).
- ¹⁹C.-J. Cheng, D. Kan, S.-H. Lim, W. R. McKenzie, P. R. Munroe, L. G. Salamanca-Riba, R. L. Withers, I. Takeuchi, and V. Nagarajan, “Structural transitions and complex domain structures across a ferroelectric-to-antiferroelectric phase boundary in epitaxial Sm-doped BiFeO₃ thin films,” *Phys. Rev. B* **80**, 014109 (2009).
- ²⁰M. Arora and M. Kumar, “Electron spin resonance probed enhanced magnetization and optical properties of Sm doped BiFeO₃ nanoparticles,” *Mater. Lett.* **137**, 285 (2014).
- ²¹C. Anthonyraj, M. Muneeswaran, S. Gokul Raj, N. V. Giridharan, V. Sivakumar, and G. Senguttuvan, “Effect of samarium doping on the structural, optical and magnetic properties of sol-gel processed BiFeO₃ thin films,” *J. Mater. Sci.: Mater. Electron.* **26**, 49 (2015).
- ²²Z. Hu, D. Chen, S. Wang, N. Zhang, L. Qin, and Y. Huang, “Facile synthesis of Sm-doped BiFeO₃ nanoparticles for enhanced visible light photocatalytic performance,” *Mater. Sci. Eng. B* **220**, 1 (2017).
- ²³M. T. Kebede, V. Dillu, S. Devi, and S. Chauhan, “Phase transition and optical properties of samarium-doped BiFeO₃ nanoparticles,” *J. Mater. Sci.: Mater. Electron.* **31**, 19950 (2020).

- ²⁴Y. Gu, Y. Zhou, W. Zhang, C. Guo, X. Zhang, J. Zhao, Y. Zhang, and H. Zheng, "Optical and magnetic properties of Sm-doped BiFeO₃ nanoparticles around the morphotropic phase boundary region," *AIP Adv.* **11**, 045223 (2021).
- ²⁵F. F. Orudzhev, N. M.-R. Alikhanov, S. M. Ramazanov, D. S. Sobola, R. K. Murtazali, E. H. Ismailov, R. D. Gasimov, A. S. Aliev, and Ş. Tãlu, "Morphotropic phase boundary enhanced photocatalysis in Sm doped BiFeO₃," *Molecules* **27**, 7029 (2022).
- ²⁶R. Alcaraz de la Osa, I. Iparragirre, D. Ortiz, and J. M. Saiz, "The extended Kubelka-Munk theory and its application to spectroscopy," *ChemTexts* **6**, 2 (2020).
- ²⁷J. D. Lindberg, "Absolute diffuse reflectance from relative reflectance measurements," *Appl. Opt.* **26**, 2900 (1987).
- ²⁸E. L. Simmons, "Diffuse reflectance spectroscopy: A comparison of the theories," *Appl. Opt.* **14**, 1380 (1975).
- ²⁹E. L. Simmons, "Reflectance spectroscopy: Application of the Kubelka-Munk theory to the rates of photoprocesses of powders," *Appl. Opt.* **15**, 951 (1976).
- ³⁰X. Bai, J. Wei, B. Tian, Y. Liu, T. Reiss, N. Guiblin, P. Gemeiner, B. Dkhil, and I. C. Infante, "Size effect on optical and photocatalytic properties in BiFeO₃ nanoparticles," *J. Phys. Chem. C* **120**, 3595 (2016).
- ³¹F. Meggle, M. Viret, J. Kreisel, and C. A. Kuntscher, "Temperature-dependent photo-response in multiferroic BiFeO₃ revealed by transmission measurements," *J. Appl. Phys.* **125**, 114104 (2019).
- ³²X. S. Xu, T. V. Brinzari, S. Lee, Y. H. Chu, L. W. Martin, A. Kumar, S. McGill, R. C. Rai, R. Ramesh, V. Gopalan, S. W. Cheong, and J. L. Musfeldt, "Optical properties and magnetochromism in multiferroic BiFeO₃," *Phys. Rev. B* **79**, 134425 (2009).
- ³³C. Hill, M. C. Weber, J. Lehmann, T. Leinen, M. Fiebig, J. Kreisel, and M. Guennou, "Role of the ferroelastic strain in the optical absorption of BiVO₄," *APL Mater.* **8**, 081108 (2020).
- ³⁴R. Palai, R. S. Katiyar, H. Schmid, P. Tissot, S. J. Clark, J. Robertson, S. A. T. Redfern, G. Catalan, and J. F. Scott, " β phase and $\gamma - \beta$ metal-insulator transition in multiferroic BiFeO₃," *Phys. Rev. B* **77**, 014110 (2008).
- ³⁵M. C. Weber, M. Guennou, C. Toulouse, M. Cazayous, Y. Gillet, X. Gonze, and J. Kreisel, "Temperature evolution of the band gap in BiFeO₃ traced by resonant Raman scattering," *Phys. Rev. B* **93**, 125204 (2016).
- ³⁶D. Sando, Y. Yang, E. Bousquet, C. Carrétéro, V. Garcia, S. Fusil, D. Dolfi, A. Barthélémy, P. Ghosez, L. Bellaiche, and M. Bibes, "Large elasto-optic effect and reversible electrochromism in multiferroic BiFeO₃," *Nat. Commun.* **7**, 10718 (2016).
- ³⁷V. Železný, D. Chvostová, D. Šimek, F. Máca, J. Mašek, N. Setter, and Y. Hong Huang, "The variation of PbTiO₃ bandgap at ferroelectric phase transition," *J. Phys.: Condens. Matter* **28**, 025501 (2016).
- ³⁸CERN Data Centre & Invenio, Zenodo, (accessed 31 July 2025), <https://doi.org/10.5281/zenodo.15175369>